Tracks of swift heavy ions in graphite studied by scanning tunneling microscopy

J. Liu,[1,2,*] R. Neumann,[1] C. Trautmann,[1,*] and C. Müller[1]
[1]*Gesellschaft für Schwerionenforschung (GSI), Planckstrasse 1, 64291 Darmstadt, Germany*
[2]*Institute of Modern Physics, Chinese Academy of Sciences (CAS), Lanzhou 730000, China*
(Received 13 February 2001; published 25 October 2001)

Tracks of energetic heavy ions on the surface and in the bulk of highly oriented pyrolytic graphite were investigated by scanning tunneling microscopy. Ni, Zn, Xe, and U ions in the MeV to GeV energy range create hillock-like damage zones with diameters between 2 and 3.5 nm, occasionally surrounded by oriented superstructures. Even at highest energy loss, tracks are formed much easier on the sample surface than in the bulk. Tracks on the original surface are generated by electronic energy loss processes above a critical threshold of 7.3 ± 1.5 keV/nm. In a transition regime from 9 to 18 keV/nm, there exists a large discrepancy between the number density of detected tracks and ion fluence. A probability of one is only found for an energy loss above about 18 keV/nm. It is concluded that tracks do not consist of a continuous cylindrical damage trail but of a discontinuous sequence of perturbed zones, in which the lattice is destroyed. Specific material properties and possible recrystallization processes are discussed.

DOI: 10.1103/PhysRevB.64.184115 PACS number(s): 81.05.Uw, 68.37.Ef, 61.80.Jh

I. INTRODUCTION

Damage in highly oriented pyrolytic graphite (HOPG), induced by ion irradiation, has been the subject of numerous studies, applying many different techniques including Rutherford back scattering, electron spin resonance, photoelectron and Raman spectroscopy, electron microscopy, and scanning tunneling microscopy.[1–3] A major reason for this enormous interest is the usage of graphite as a moderating and shielding material for nuclear reactors.

HOPG crystallizes in a hexagonal, layer-type lattice. The distance of 0.335 nm between adjacent sheets is considerably greater than the shortest interatomic distance of 0.142 nm within a plane. The layers are held together by van der Waals forces, whereas the atoms within a plane have planar covalent bonds. The lamellar structure gives rise to highly anisotropic physical properties, e.g., high thermal conductivity ($\lambda \sim 30$ W/cm K) and semimetallic electrical conductivity (resistivity $\rho \sim 4 \times 10^{-5}\ \Omega$ cm) parallel to the layers, but poor conductivity ($\lambda \sim 0.06$ W/cm K, $\rho \sim 5 \times 10^{-3}\ \Omega$ cm) normal to the planes. HOPG can easily be cleaved providing surfaces atomically smooth over hundreds of nanometers. Scanning tunneling microscopy (STM) allows imaging of such surfaces with resolution of the lattice order, even in ambient air.

In the past, many groups used STM to record nanometer-sized defects induced when exposing HOPG surfaces to various ion beams.[4] Most investigations deal with projectiles in the eV to keV energy regime where the stopping process of the ions is dominated by elastic collisions with the target atoms.[5–19] Only some studies have been performed with swift ions of several MeV per nucleon (MeV/u), which deposit their energy mainly by inelastic collisions with target electrons, thereby causing excitation and ionization processes.[20–25] When studying track formation in HOPG, the specific material properties due to the layered structure of graphite have to be taken into account. If the ion irradiation is performed perpendicular to the planes, the primarily deposited energy may be more quickly dissipated radially from the ion path by π electrons between the layers having efficiency similar to a metal. Of particular interest is the open question whether the large energy deposition in electronic stopping processes leads to track formation not only on the surface but also in the bulk. Note that up to now, no tracks of any kind could be found in bulk samples by means of transmission electron microscopy (TEM), neither by phase nor by diffraction contrast.[26,27]

In this work, our main effort focuses on imaging tracks of various heavy ion species with MeV-GeV energies by means of STM. We present a systematic study of the creation probability and mean size of the tracks as a function of electronic energy loss, studying the original HOPG surface and in some cases also deeper crystal layers.

II. EXPERIMENT

The experiments were performed using cleaved HOPG with (0001) orientation, supplied by Union Carbide or Advanced Ceramics. The samples were irradiated by defocused Ni, Zn, Xe, and U ion beams with an initial kinetic energy of 11.4 MeV/u at the linear accelerator (UNILAC), and with Zn ions of 1.4 MeV/u at the high charge injector (HLI) of GSI, Darmstadt. All irradiations were performed at room temperature under normal incidence up to a fluence between 1.3×10^{11} and 1.8×10^{12} ions/cm^2, and with a flux around 4×10^8 ions/(cm^2 s) for the Xe ions and lower for other ion species. At the beamline of the UNILAC, a detector with three thin Al foils (total thickness 2.7 μm) is positioned in front of the samples in order to control the fluence during the irradiation. For this purpose, the yield of secondary electrons from the detector is recorded and calibrated by means of a Faraday cup. After passing the foils, the projectiles have reached equilibrium charge state when impinging on the sample surface. The applied fluence was additionally cross-checked by chemical track etching of simultaneously irradiated polymer test samples. Counting the number density of etched pores under a scanning electron microscope, the fluence was determined with an accuracy of 10–20 %.

TABLE I. Irradiation parameters. E is the kinetic energy of the ions when entering the sample surface. S_e and S_n denote the electronic and nuclear energy loss, respectively, as calculated with the TRIM 92 code. The track diameters D and the creation yield are given for results on the original sample surface.

Ions	E[a] (MeV)	Degrader (μm)	S_e (keV/nm)	S_n ($\times 10^{-2}$) (keV/nm)	Range (μm)	D (nm)	Yield %
^{58}Ni	651		5.1	0.3	97.6		
	600	10.0	5.3	0.3	87.8		0.6
	504	28.0	5.8	0.3	70.4		1.3
	298	61.3	7.2	0.5	38.2	2.2	2.2
	113	85.5	9.2	1.3	15.3	2.2	12.7
^{70}Zn	783		5.7	0.3	106.8	2.1	0.3
	356	66.5	7.9	0.6	42.7	2.2	2.3
	197	86.0	9.3	1.0	23.8	2.3	11.8
	109	95.6	10.0	1.7	14.7		
	98[b]		10.0	1.8	13.6	2.1	
^{132}Xe	1469		13.8	0.9	93.7	2.3	15.3
	789	46.7	16.5	1.6	48.3	2.5	39.1
	482	65.4	17.8	2.5	30.5	2.5	60.0
^{136}Xe	1514		13.8	0.9	96.6	1.9	17.9
	475	68.7	17.8	2.5	30.2	2.1	55.8
	300	79.1	17.8	3.8	20.4	2.4	84.2
^{138}U	2636		27.6	2.5	101.2	3.5	
	1159	52.9	29.7	5.1	50.0	3.1	110.0
	192	90.9	20.4	22.0	14.5	2.8	
	108	96.0	16.3	35.0	10.0		
^{238}U	2636		27.6	2.5	101.2	3.0	
	1190	51.8	29.7	5.0	51.1	3.0	99.2
	534	75.8	27.1	9.7	28.4	3.3	72.3
	326	84.4	24.4	15.6	20.4	3.0	80.5

[a]The accuracy of the energy is 10–20 % and mainly determined by the uncertainties of the TRIM code.
[b]For the irradiation at the HLI, the charge state of the ions was not in equilibrium but had a value of $+10e$.

In most cases, aluminum degraders of different thickness were placed in front of the samples in order to modify the energy and thereby the stopping power of the projectiles. The projected ion range was always much smaller than the sample thickness. The parameters of different irradiation experiments are presented in Table I. The values of the ion energy behind the degrader, the electronic (S_e) and nuclear (S_n) energy loss and of the range were calculated with the TRIM 92 code.[28] It should be emphasized, though, that this code refers to bulk calculations of random targets and is not capable of properly handling anisotropic materials and orientation effects such as channeling.

The irradiated samples were investigated using a home-built STM.[29,30] The tunneling tips were mechanically prepared from thin Pt/Ir wires. Their imaging quality was repeatedly checked on nonirradiated regions of the same sample. The microscope was operated in ambient conditions, using constant current mode with a bias voltage typically 250 mV, tunneling current 1 nA, and scan rate 3 Hz.

Tracks were studied on the original sample surface and, in some selected cases, in the bulk by cleaving off thin layers with an adhesive tape. During the cleavage process, the sample remained mounted on the STM holder in a slightly withdrawn position. By reading the z position of the sample on a micrometer of the microscope, before and after cleaving, with the tip having contact to the sample surface, we could measure the thickness of the removed layer with an estimated accuracy of about ± 1 μm.

III. TRACK OBSERVATIONS

STM images of samples irradiated with U ions (1.19 GeV) and Xe ions (482 MeV) are presented in Fig. 1 showing stochastically distributed and well-isolated features on the initially flat surface. The bright areas correspond to hillocks protruding from the sample surface, whereas the dark shadowlike zones on the right side of each hillock are ascribed to an electronic artifact related to the scanning feedback loop of the microscope (the shadows appear on the left side when reversing the scanning direction).

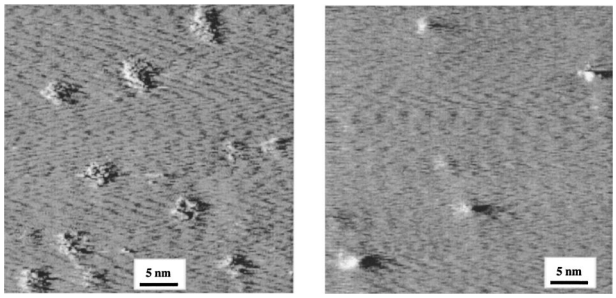

FIG. 1. STM micrographs obtained from graphite surfaces irradiated with (left) 7.9×10^{11} U ions/cm^2 (1.19 GeV) and (right) 4.3×10^{11} Xe ions/cm^2 (482 MeV). The fast scanning was performed along the horizontal direction.

STM images at even higher resolution are shown for the same ion species in Fig. 2. Each of these protrusions is surrounded by the undisturbed crystal with a lattice constant 0.246 nm, typical of the hexagonal graphite structure. Within the track areas, the lattice is disrupted to an extent that atomic resolution can no longer be obtained.

The geometrical shape of most of the impact regions is rather irregular. In particular for U ions, the tracks look like agglomerates of smaller damage zones.

Our track observations are very similar for all ion species and energies except for samples that were covered during irradiation with a degrader of thickness 90 μm or larger. In that situation, many significantly smaller defects appear, sometimes as loose agglomerates, in other cases as satellites in close proximity of a larger defect (Fig. 3). Assuming that each ion produces an individual track, the scan in Fig. 3 should, for statistical reasons, contain about three ion impacts only. Considering known discrepancies of 10–20 % between the TRIM code and experimental data,[31,32] we assume that this kind of damage originates from a region close to the stopping end of the ions, where elastic collisions with the target atoms dominate. Since unambiguous identification of single tracks is not possible for this situation, such images were not further analyzed.

Our findings that energetic ions create protrusions instead of craters are in accordance with observations of many other groups using light or heavy ions in a wide energy regime between 50 eV and several GeV.[5–24] These protrusions are

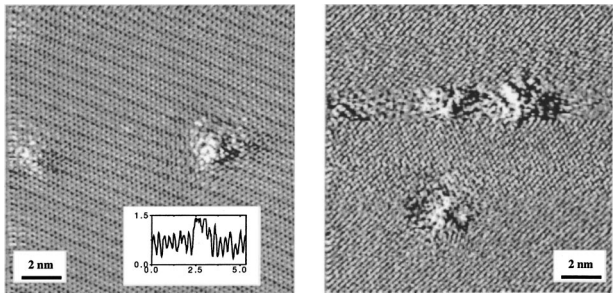

FIG. 2. High-resolution STM images of a HOPG surface bombarded with (left) Xe ions of 1.51 GeV and (right) U ions of 1.19 GeV. The inset shows a height profile from left to right across the Xe ion track next to it (scale of axes in nm).

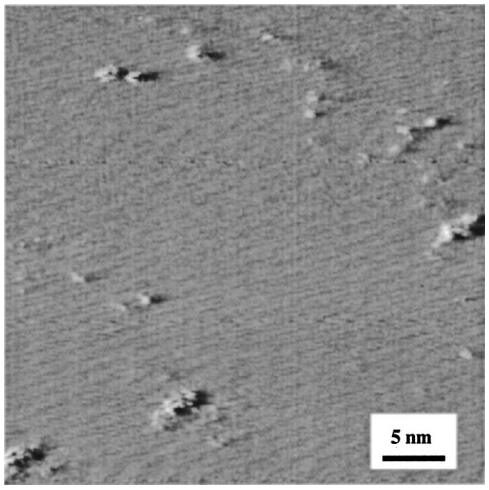

FIG. 3. STM image of tracks induced by U ions of 108 MeV. The fluence was 2×10^{11} ions/cm^2.

commonly interpreted topographically because a variation of tip material, tip polarity, and bias voltage did not noticeably influence the STM images. It is assumed that changes of the local density of electronic states contribute only to a smaller extent to the measured height.[7,13]

Another interesting observation concerns the appearance of superstructures occasionally imposed on the regular graphite lattice in the close surroundings of the protrusions. Such patterns appear for all different ion species on the original surface as well as in deeper layers exposed by cleavage. They have a periodicity of $(\sqrt{3}\times\sqrt{3})\,R$ (R is the interatomic distance of 0.246 nm along the [1100] direction) and are rotated by about 30° with respect to the underlying graphite lattice. Figure 4 gives two examples of superstructures showing that several different orientations can coexist continuously merging into each other. They gradually decay from the center of the hillocks, typically within a distance of 1–3 nm. It should be remarked that several groups have observed such structures in the close surroundings of different features such as adsorbed atoms,[33–35] defects,[36] grain boundaries,[37] and ion tracks.[7,9,21] The patterns were ascribed to the interference of incident and scattered Bloch waves of the quasi-free electrons in the graphite surface layer.[33,38]

For a quantitative examination of the track dimensions, the images were analyzed by drawing height profiles (cf.

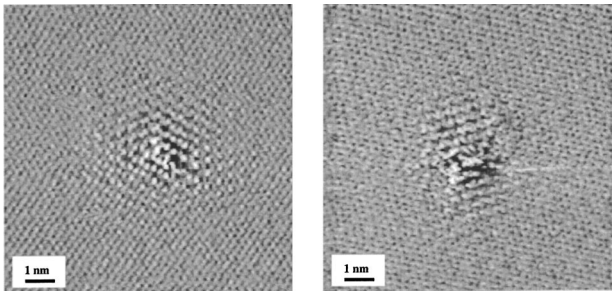

FIG. 4. High resolution STM images showing superstructures surrounding the tracks of Xe ions of 1.47 GeV (left) and U ions of 192 MeV (right).

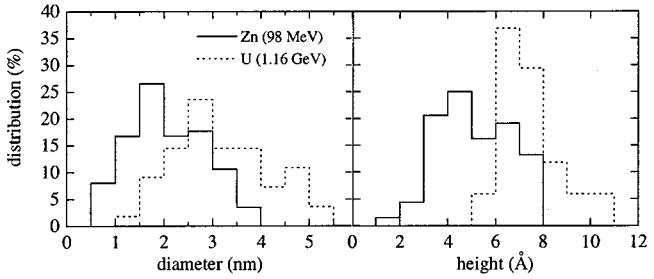

FIG. 5. Histograms of track diameters (left) and heights (right) of Zn (98 MeV) and U (1.16 GeV) ions.

inset of Fig. 2) across several tens and sometimes even up to hundreds and more protrusions. The diameter was defined by the two foot points where the vertical track contour merges with the horizontal baseline of the undamaged surface. Because of the irregular shape of the hillocks, height profiles along two different directions were taken from each protrusion. In Fig. 5, diameter and height histograms are presented for 98 MeV Zn and 1.16 GeV U ions. Mean values and full widths at half maximum (FWHM) were determined by fitting a Gaussian curve to each histogram. The mean height of the protrusion of Zn and U ions is approximately 0.5 ± 0.4 nm and 0.7 ± 0.3 nm. The respective diameters are 2 and 3 nm, both exhibiting a rather large dispersion of FWHM $\sim$2 nm.

A complete data set of the mean track diameter as a function of the energy loss is given in Fig. 6. The data points for Ni, Zn, and Xe ions scatter around 2 nm whereas the diameters for U ions show a slight increase as a function of S_e up to a maximum of 3.5 nm.

While the data described up to now were recorded on the original sample surface, we also imaged tracks from deeper bulk layers by cleaving thin slices from crystals irradiated with U ions of 2.64 GeV. In general, the tracks observed in these bulk layers are very similar to the features found on the original surface. Hillocks are found on both adjacent lattice planes that are exposed by cleavage. The mean track diameters for these samples decreased from 3.0(1) nm at the original surface to 2.6(1) nm and 2.2(1) nm at a sample depth of around 5 and 40 μm, respectively.

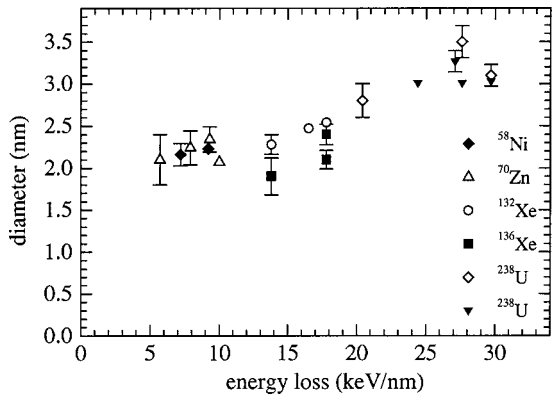

FIG. 6. Average track diameter as a function of energy loss. Tracks below 9 keV/nm are ascribed to nuclear collision processes (cf. data analysis). The errors correspond to one standard deviation (errors with the size of symbols are not shown).

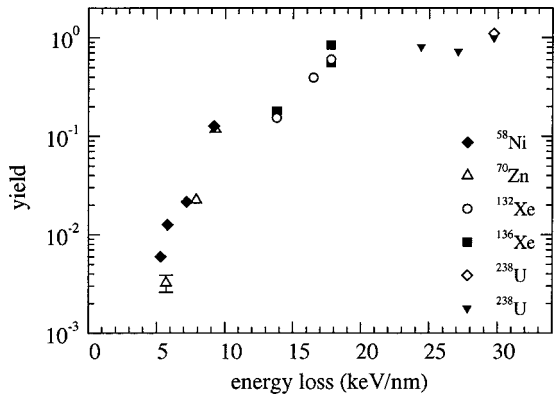

FIG. 7. Track creation yield ξ on the original HOPG surface versus the electronic energy loss on a semilogarithmic scale. The error of ξ is determined by the fluence uncertainty of 10–20 %.

IV. DATA ANALYSIS

A. Track creation yield

For all samples, the number density of observed protrusions N_t compared to the applied ion fluence Φ was analyzed systematically. On the original sample surface, the probability of track creation, defined as yield $\xi = N_t/\Phi$, as a function of the energy loss varies over several orders of magnitude (Fig. 7). A one-to-one relation has been found only for ions of highest electronic energy loss which is in agreement with data of Bouffard *et al.*[21] for U ions of 671 MeV ($S_e = 27.7$ keV/nm). Below an energy loss of about 18 keV/nm, the yield decreases significantly and reaches extremely small values around 5 keV/nm for Ni and Zn ions. It should be noted that the yield data of the irradiation with 2.64 GeV U and 98 MeV Zn ions was discarded due to fluence uncertain-

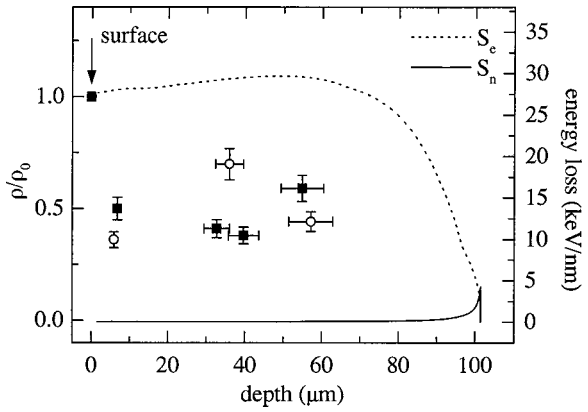

FIG. 8. Area density of tracks in the bulk ρ compared to that on the original surface ρ_0 as a function of depth in the bulk. For STM imaging, the interfaces were exposed by cleaving off thin layers from two different crystals (full symbols and open symbols) irradiated with U ions of 2.64 GeV. Superimposed is the electronic (S_e) and the nuclear (S_n) energy loss.

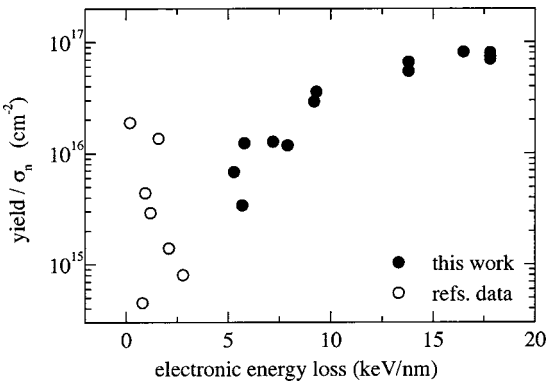

FIG. 9. Yield normalized by nuclear cross section versus the electronic energy loss. The open symbols correspond to data from Refs. 14, 17, and 22.

ties. Some of the low-energy data was also not included because of difficulties in identifying the tracks reliably (cf. Fig. 3).

Compared to the original surface, the probability of track formation is significantly reduced in deeper bulk layers. Figure 8 shows the area density of tracks in the bulk ρ divided by that on the original surface ρ_0 versus depth in the bulk. The decrease of ρ/ρ_0 contrasts with the fact that the energy loss in deeper layers is almost identical or even higher than on the original surface.

B. Surface track formation threshold

The yield as a function of the electronic energy loss allows us to determine a threshold for track creation on the HOPG surface. In the following analysis, we ignored data with $S_e > 18$ keV/nm, because in this regime the yield is close to 100%. Although the stopping power of the projectiles used in our study is dominated by electronic processes, we have to discuss possible contributions of nuclear collisions. Using the TRIM code,[28] the nuclear cross section σ_n of each ion species was calculated for the surface layer assuming a displacement energy of 35 eV.[39] In Fig. 9, the experimental yield divided by σ_n is shown as a function of electronic energy loss. Displayed are also yield data from other groups[14,17,21,22] where the ion beams are mainly characterized by dominant nuclear stopping. These yield data (open symbols) normalized by σ_n reach maximum values around $2\times10^{16}\,\mathrm{cm}^{-2}$. This tells us that nuclear collisions could explain the low yield for some of the high-energy ions, such as Ne ions of 215 MeV ($S_e = 0.8$ keV/nm),[22] and in our case the five data points (Ni and Zn ions) with S_e below 9 keV/nm. For ions with $S_e > 9$ keV/nm, the yield/σ_n values are much higher and the observed damages can unambiguously ascribed to electronic processes. Concentrating on electronic effects, we therefore excluded ions with $S_e \leqslant 9$ keV/nm, since the damage process is dominated by S_n.

From a linear fit of the yield data between 9 and 18 keV/nm, a critical $S_e = 7.3 \pm 1.5$ keV/nm is deduced from the intersection with the abscissa. Finally, it should be emphasized that this threshold concerns track formation at the sample surface and not in the bulk material, where the creation yield is significantly reduced.

V. DISCUSSION

The appearance of hillocks observed on the original sample surface reflects the creation of defects or defect clusters. For a volume expansion, we suppose that mainly interstitials contribute because they lie between the lattice planes and easily aggregate due to their high mobility parallel to the lattice planes.[40–42] According to Refs. 10 and 13, vacancies can probably be neglected since they are located in the lattice planes, have a low mobility at room temperature, and cause no volume increase of the crystal. Furthermore, we have to consider that the damage embedded in the lattice along the ion path develops interplanar stress leading to an expansion along the *c* axis towards the surface area around the impact site. The hillocks we observe on the two adjacent lattice planes of the crystal (exposed by cleavage) are a clear indication that the stress stored in the bulk relaxes to these new surfaces.

Another remarkable result are the small diameters of the tracks between 2 and 3.5 nm and heights of a fraction of a nanometer. Compared to other lamellar crystals, such as mica and germanium sulfide, the track diameters in graphite are smaller by more than a factor of 2. For the energy loss regime considered here, track diameters in mica as measured by TEM vary from 4 to about 10 nm.[43] Note, though, that all ion-induced hillocks, reported so far, have similar small dimensions. Obviously, neither the ion species nor the stopping mechanism has a strong influence on the extension of the damage.

Summarizing the analysis of the complete set of our track data, the following two findings are most remarkable: (1) the large discrepancy of the probability of track creation on the sample surface compared to bulk material, and (2) the strong S_e dependence of the creation yield in the regime between 7 and 18 keV/nm. Both phenomena can be understood if we assume a morphology consisting of a discontinuous sequence of damage segments instead of a homogeneous cylinder. Due to the stochastic nature of the linear energy transfer, the critical energy density to create extensive damage is probably surpassed only occasionally and not along the full length of the ion path. These fluctuations are also reflected in the large dispersion of the hillock diameters (cf. Fig. 5), and have been observed for ion irradiations at energy losses close to the threshold.[44–49] The S_e dependence of the yield can be understood if we assume that the gaps between two adjacent damage segments decrease with increasing energy loss.

For Xe or lighter ions, the track size seems to be constant and does not depend on the electronic energy loss (cf. Fig. 6). An increase is only significant for U ions above 18 keV/nm, the same critical value where the track creation yield reaches a value around 100%. The phenomenon of constant diameters has also been seen in other insulators such as yttrium-iron garnet and lithium fluoride[50,51] for low stopping powers. It is possibly linked to the discontinuous nature of the tracks where a single defect segment needs a critical minimum size to be stable.

Finally, it should be mentioned that the discontinuous damage morphology may explain why no tracks could be

found by means of TEM.[52,53] Probably, discontinuous tracks with diameters of 2–3 nm are extremely difficult to identify with TEM.

In order to understand the small track dimensions, we have to consider the partly metallic character of graphite. It is reasonable to assume that the incident ion creates a primary excited zone of cylindrical shape. In the crystal planes, the energy deposited by the projectile is dissipated by the electrons very efficiently. However, some of the energy is transferred to the atoms of the lattice initiating atomic motion which finally may result in a phase change from the crystalline to the amorphous state. Since graphite is a monoatomic crystal, we certainly have to consider that the disordering of the lattice is followed in time by a rapid recrystallization occurring in particular in the bulk. On the surface, such a process is expected to be less pronounced, because the binding symmetry is broken and effects such as electron emission or sputtering may play a crucial role.

For a better understanding of the track formation process, some preliminary thermal spike calculations were performed.[54] Due to the special material properties of the lamellar structure, graphite was treated as a metal. For a reasonable set of relevant parameters (e.g., thermal conductivity, electron-phonon coupling constant), the model is able to describe our experimental threshold for track creation. However, the absolute values of the diameters are always by a factor of 2 too large. This is surprising insofar that this model has given a rather good description of experimental track observations for many materials, in particular for metals.[55–59] Since the thermal spike approach does not take into account recrystallization effects, the discrepancy is possibly another indication that in graphite, epitaxial regrowth is involved during track formation. Finally, it should be pointed out that recrystallization is also favored for other monoatomic tetrahedrally bonded systems such as diamond, Si, and Ge, for which GeV heavy ions do not generate latent tracks. A more detailed discussion related to structural, bonding, and/or defect mobility characteristics is given in Refs. 60 and 61.

VI. CONCLUSIONS

The high resolution of STM has enabled us to investigate in detail the damage induced by different species of swift heavy ions on the surface as well as in the bulk of HOPG. In some cases, the impact zones are surrounded by a lattice superstructure consisting of parallel and equidistant straight lines ascribed to long-distance electronic perturbation caused by the defect. Compared to tracks in many other materials, the hillocks created in HOPG are characterized by particularly tiny dimensions (average height between 0.3 and 0.9 nm and mean diameters between 2 and 3.5 nm).

Concerning the formation of ion tracks in graphite, the following findings are most striking. (1) Even at highest energy loss, tracks are formed much easier on the surface than in the bulk. (2) Tracks on the original surface are created by electronic energy loss processes above a critical threshold of 7.3 ± 1.5 keV/nm. (3) In a transition regime from 9 to 18 keV/nm, there exists a large discrepancy between the number density of detected tracks and ion fluence. A probability of one is only found for energy loss above about 18 keV/nm. It is concluded that tracks do not consist of a continuous cylindrical damage trail but of a discontinuous sequence of perturbed zones, in which the lattice is destroyed.

ACKNOWLEDGMENTS

We would like to thank L. Chadderton, K. Schwartz, and M. Toulemonde for many fruitful discussions, and S. Grafström, A. Müller, R. Spohr, and J. Vetter for help during irradiation experiments and at the microscope. This project was supported by the National Science Foundation of China (10075064). J.L. gratefully acknowledges the support of M. D. Hou and Y. F. Jin, and financial help from the CAS and from the GSI during the stay in Germany.

*Corresponding authors. FAX: +49 6159 712179. Email addresses: C.Trautmann@gsi.de and J.Liu@gsi.de

[1] M. S. Dresselhaus and R. Kalish, *Ion Implantation in Diamond, Graphite and Related Materials* (Springer, Berlin, 1992).

[2] B. S. Elman, M. Shayegan, M. S. Dresselhaus, H. Mazurek, and G. Dresselhaus, Phys. Rev. B **25**, 4142 (1982).

[3] *Nuclear Graphite*, edited by R. Nightingale (Academic, London, 1982).

[4] R. Neumann, Nucl. Instrum. Methods Phys. Res. B **151**, 42 (1999).

[5] L. Porte, M. Phaner, C. H. de Villeneuve, N. Moncoffre, and J. Tousset, Nucl. Instrum. Methods Phys. Res. B **44**, 116 (1989).

[6] R. Coratger, A. Claverie, F. Ajustron, and J. Beauvillain, Surf. Sci. **227**, 7 (1990).

[7] L. Porte, C. H. de Villeneuve, and M. Phaner, J. Vac. Sci. Technol. B **9**, 1064 (1991).

[8] T. Li, B. V. King, R. J. MacDonald, G. F. Gotterill, D. J. O'Connor, and Q. Yang, Surf. Sci. **312**, 399 (1994).

[9] Juejue Yan, Zhigang Li, Chuangyong Bai, W. S. Yang, Yugang Wang, Weijiang Zhao, Yixiu Kang, F. C. Yu, Pengji Zhai, and Xiaowei Tang, J. Appl. Phys. **75**, 1390 (1994).

[10] K. P. Reimann, W. Bolse, U. Geyer, and K. P. Lieb, Europhys. Lett. **30**, 463 (1995).

[11] D. Marton, H. Bu, K. J. Boyd, S. S. Todorov, A. H. Al-Bayati, and J. W. Rabalais, Surf. Sci. **326**, L489 (1995).

[12] J. R. Hahn and H. Kang, Surf. Sci. **357-358**, 165 (1996).

[13] W. Bolse, K. Reimann, U. Geyer, and K. P. Lieb, Nucl. Instrum. Methods Phys. Res. B **118**, 488 (1996).

[14] Hisato Ogiso, Shizuka Nakano, Hiroshi Tokumoto, and Kazushi Yamanaka, in *Ion-Solid Interactions for Materials Modification and Processing*, edited by D. B. Poker, D. Ila, Y-S. Cheng, L. R. Hamott, and T. W. Sigmon, Mater. Res. Soc. Symp. Proc. No. 396 (MRS, Pittsburgh, 1996), p. 667.

[15] T. Seki, T. Kaneko, D. Takeuchi, T. Aoki, J. Matsuo, Z. Insepov, and I. Yamada, Nucl. Instrum. Methods Phys. Res. B **121**, 498 (1997).

[16] Sönke Habenicht, Wolfgang Bolse, and Klaus-Peter Lieb, Rev. Sci. Instrum. **69**, 2120 (1998).

[17] Yugang Wang, Yixiu Kang, Weijiang Zhao, Sha Yan, Penji Zhai, and Xiaowei Tang, J. Appl. Phys. **83**, 1341 (1998).

[18] J. R. Hahn and H. Kang, Phys. Rev. B **60**, 6007 (1999).
[19] T. Matsukawa, S. Suzuki, T. Fukai, I. Ohdomari, and T. Tanaka, Appl. Surf. Sci. **107**, 227 (1996).
[20] H. Kemmer, S. Grafström, M. Neitzert, M. Wörtge, R. Neumann, C. Trautmann, J. Vetter, and N. Angert, Ultramicroscopy **42-44**, 1345 (1992).
[21] S. Bouffard, J. Cousty, Y. Pennec, and F. Thibaudau, Radiat. Eff. Defects Solids **126**, 225 (1993).
[22] L. P. Biró, J. Gyulai, and K. Havancsák, Phys. Rev. B **52**, 2047 (1995).
[23] L. P. Biró, J. Gyulai, and K. Havancsák, Nucl. Instrum. Methods Phys. Res. B **112**, 270 (1996).
[24] L. P. Biró, J. Gyulai, and K. Havancsák, Nucl. Instrum. Methods Phys. Res. B **122**, 476 (1997).
[25] J. P. Singh, A. Tripathi, and D. Kanjilal, Vacuum **57**, 319 (2000).
[26] L. T. Chadderton, D. Fink, Y. Gamaly, H. Moeckel, L. Wang, and H. Omichi, Nucl. Instrum. Methods Phys. Res. B **91**, 71 (1994).
[27] A. Dunlop, G. Jaskierowicz, and L. T. Chadderton, Nucl. Instrum. Methods Phys. Res. B **145**, 532 (1998).
[28] J. F. Ziegler, J. P. Biersack, and U. Littmark, in *The Stopping and Range of Ions in Matter*, edited by J. F. Ziegler (Pergamon, New York, 1985).
[29] S. Grafström, J. Kowalski, and R. Neumann, Meas. Sci. Technol. **1**, 139 (1990).
[30] S. Grafström, J. Kowalski, R. Neumann, O. Probst, and M. Wörtge, J. Vac. Sci. Technol. A **8**, 357 (1990).
[31] C. Trautmann, K. Schwartz, and O. Geiss, J. Appl. Phys. **83**, 3560 (1998).
[32] G. S. Randhawa and H. S. Virk, Radiat. Meas. **26**, 541 (1996).
[33] H. A. Mizes and J. S. Foster, Science **244**, 559 (1989).
[34] J. Xhie, K. Sattler, U. Müller, N. Venkateswaran, and G. Raina, Phys. Rev. B **43**, 8917 (1991).
[35] G. M. Shedd and P. E. Russell, Surf. Sci. **266**, 259 (1992).
[36] J. Schneir, P. K. Hansma, V. Elings, J. Gurley, K. Wickramasinghe, and R. Sonnenfeld, J. Soc. Photo-Opt. Instrum. Eng. **897**, 16 (1988).
[37] T. R. Albrecht, H. A. Mizes, J. Nogami, Sang-il Park, and C. F. Quate, Appl. Phys. Lett. **52**, 362 (1988).
[38] J. Valenzuela-Benavides and L. Morales de la Garza, Surf. Sci. **330**, 227 (1995).
[39] H. J. Steffen, D. Marton, and J. W. Rabalais, Phys. Rev. Lett. **68**, 1726 (1992).
[40] B. T. Kelly, *Physics of Graphite* (Barking, UK, 1981).
[41] T. Iwata, J. Phys. Soc. Jpn. **33**, 1060 (1972).
[42] H. Maeta, T. Iwata, and S. Okuda, Phys. Lett. **53A**, 295 (1975).
[43] J. Vetter, R. Scholz, D. Dobrev, and L. Nistor, Nucl. Instrum. Methods Phys. Res. B **141**, 747 (1998).
[44] M. Toulemonde, N. Enault, Jin-Yun Fan, and F. Studer, J. Appl. Phys. **68**, 1545 (1990).
[45] C. Trautmann, R. Spohr, and M. Toulemonde, Nucl. Instrum. Methods Phys. Res. B **83**, 513 (1993).
[46] C. Trautmann, S. Bouffard, and R. Spohr, Nucl. Instrum. Methods Phys. Res. B **116**, 429 (1996).
[47] J. Jensen, A. Dunlop, and S. Della-Negra, Nucl. Instrum. Methods Phys. Res. B **146**, 399 (1998).
[48] C. Trautmann, K. Schwartz, J. M. Costantini, T. Steckenreiter, and M. Toulemonde, Nucl. Instrum. Methods Phys. Res. B **146**, 367 (1998).
[49] A. Müller, C. Müller, R. Neumann, and F. Ohnesorge, Nucl. Instrum. Methods Phys. Res. B **166-167**, 581 (2000).
[50] Ch. Houpert, F. Studer, D. Groult, and M. Toulemonde, Nucl. Instrum. Methods Phys. Res. B **39**, 720 (1989).
[51] C. Trautmann, M. Toulemonde, K. Schwartz, J. M. Costantini, and A. Müller, Nucl. Instrum. Methods Phys. Res. B **164-165**, 365 (2000).
[52] L. T. Chadderton, D. Fink, Y. Gamaly, H. Moeckel, L. Wang, and H. Omichi, Nucl. Instrum. Methods Phys. Res. B **91**, 71 (1994).
[53] A. Dunlop, G. Jaskierowicz, and L. T. Chadderton, Nucl. Instrum. Methods Phys. Res. B **145**, 532 (1998).
[54] M. Toulemonde (private communication).
[55] M. Toulemonde, C. Dufour, and E. Paumier, Phys. Rev. B **46**, 14 362 (1992).
[56] M. Toulemonde, Ch. Dufour, A. Meftah, and E. Paumier, Nucl. Instrum. Methods Phys. Res. B **166-167**, 903 (2000).
[57] Z. G. Wang, Ch. Dufour, E. Paumier, and M. Toulemonde, J. Phys.: Condens. Matter **6**, 6733 (1994).
[58] Z. G. Wang, Ch. Dufour, E. Paumier, and M. Toulemonde, J. Phys.: Condens. Matter **7**, 2525 (1995).
[59] M. Toulemonde, Z. Wang, E. Paumier, and Ch. Dufour, Nucl. Instrum. Methods Phys. Res. B **112**, 26 (1996).
[60] L. T. Chadderton, D. Fink, H. J. Möckel, K. K. Dwivedi, and A. Hammoudi, Radiat. Eff. Defects Solids **127**, 163 (1993).
[61] L. T. Chadderton and D. Fink, Radiat. Eff. Defects Solids **152**, 87 (2000).